

Article

Fluvial Responses to Late Quaternary Climate Change in a Humid and Semi-Humid Transitional Area: Insights from the Upper Huaihe River, Eastern China

Zongmeng Li ¹, Yixuan Wang ^{2,*}, Wenmin Zhu ¹, Hongshan Gao ³, Fenliang Liu ⁴, Wei Xing ⁵, Chenguang Zhang ¹, Qiang Qiao ¹ and Xiaoying Lei ¹

- ¹ Henan Key Laboratory for Synergistic Prevention of Water and Soil Environmental Pollution, School of Geographic Sciences, Xinyang Normal University, Xinyang 464000, China; lizm@xynu.edu.cn (Z.L.)
- ² Key Laboratory of Comprehensive and Highly Efficient Utilization of Salt Lake Resources, Qinghai Institute of Salt Lakes, Chinese Academy of Sciences, Xining 810008, China
- ³ Key Laboratory of Western China's Environmental Systems (Ministry of Education), College of Earth and Environmental Sciences, Lanzhou University, Lanzhou 730000, China
- ⁴ School of Municipal and Surveying Engineering, Hunan City University, Yiyang 413000, China
- ⁵ National Park Research Center, Sanming University, Sanming 365004, China
- * Correspondence: yixuanwang@isl.ac.cn

Abstract: Research into river processes in different climatic and geomorphic areas is vital for a clearer understanding of the non-linear responses of rivers to climate change. The Huaihe River (HHR) Basin, located in China's North–South Transition Zone (NSTZ), provides an ideal environment in which to explore river responses to climate change within a humid/semi-humid transitional area. Based on optically stimulated luminescence (OSL) and ¹⁴C dating, combined with sedimentary stratigraphic analyses, we reconstructed the river processes of three sedimentary sequences in the upper HHR since the Late Quaternary. Our results showed that the upper HHR was characterized by aggrading meandering channels from the Last Glacial Maximum (LGM) to 0.5 ka, and an aggrading wandering channel from 0.2 ka to the present. Two periods of downcutting occurred during 5.8–3.0 and 0.5–0.2 ka, respectively. The river incision is potentially linked to changes in the climate during the Mid–Late Holocene transition and the Little Ice Age (LIA). However, there have been no marked changes in channel patterns in the upper HHR since the LGM. This phenomenon reflects the influence of vegetation on channel patterns during climate change. Our results showed that the fluvial processes in different climatic and geomorphic areas are controlled by the local hydroclimatic regime.

Keywords: fluvial process; climate change; Late Quaternary; upper Huaihe River



Citation: Li, Z.; Wang, Y.; Zhu, W.; Gao, H.; Liu, F.; Xing, W.; Zhang, C.; Qiao, Q.; Lei, X. Fluvial Responses to Late Quaternary Climate Change in a Humid and Semi-Humid Transitional Area: Insights from the Upper Huaihe River, Eastern China. *Water* **2023**, *15*, 1767. <https://doi.org/10.3390/w15091767>

Academic Editor: Achim A. Beylich

Received: 21 March 2023

Revised: 30 April 2023

Accepted: 30 April 2023

Published: 4 May 2023



Copyright: © 2023 by the authors. Licensee MDPI, Basel, Switzerland. This article is an open access article distributed under the terms and conditions of the Creative Commons Attribution (CC BY) license (<https://creativecommons.org/licenses/by/4.0/>).

1. Introduction

Fluvial responses to climate change and other impact factors are one of the key issues in fluvial geomorphology [1–9]. Of these multiple impact factors, climate change has the capacity to control river behavior by directly and indirectly affecting river runoff and sediment supply [10–13]. Especially in the context of global warming, combined with frequent extreme climatic events or abrupt climate change, how to explore the complexity of river responses to climate change (or extreme climate events in particular) has become an important issue for fluvial geomorphologists.

Many regional and global syntheses of fluvial processes have shown that, in the long term (i.e., 10–1000 kyr), fluvial activities are driven by the orbital-scale climate fluctuations overprinted on to the effects of tectonic uplift [2,3,6,14–16]. However, in the short term (i.e., 1–10 kyr), there remains considerable debate about how rivers respond to climate change [4,17–19]. The modeled “non-linear” responses of rivers to short-term climate change have been confirmed over recent decades by many studies based on syntheses of

research into different climatic regions [1,4,11,20,21]. This “non-linear” model comprehensively considers the feedback regulation exerted by vegetation cover, soil cohesion, and other factors on climate change, and it emphasizes the impact of climate transitions on river behavior, i.e., river incision, the formation of terraces, and changes in fluvial style. It has become evident that such changes occur mainly during periods of climatic transition (cold–warm or warm–cold), while in the non-transitional periods (cold or warm), river behavior is relatively stable [4,5,11,22–25]. However, many studies have suggested that river processes in different regions may respond differently to climate change in terms of their diversity and complexity [12,17–19,24,26]. These differences may be related to the local climate, topography, vegetation, and internal adjustments of the river system [1,4,12,17,26]. It is, therefore, necessary to improve the comparative study of river processes in different regions.

The Huaihe River (HHR), which is one of the largest rivers in Eastern China, is located in China’s North–South Transitional Zone (NSTZ) (Figure 1). The NSTZ, which lies roughly along the Qinling Mountains–Huaihe River axis, is the transition zone between China’s humid and semi-humid zones, as well as the warm temperate and north subtropical zones [27]. This area is transitional and, therefore, sensitive to changes in its river systems, climate, and other natural, environmental factors [28]. The NSTZ, therefore, provides an excellent experimental region in which to explore fluvial processes within a humid and semi-humid transitional area. Field investigations showed that there are well-developed sedimentary outcrops on both sides of the upper HHR. Based on sedimentary analyses, and ^{14}C and optically stimulated luminescence (OSL) dating, the fluvial geomorphic processes of the upper HHR were established. Subsequently, we discussed the fluvial responses to climate change in our chosen study area, and the non-linear responses of rivers to climate change.

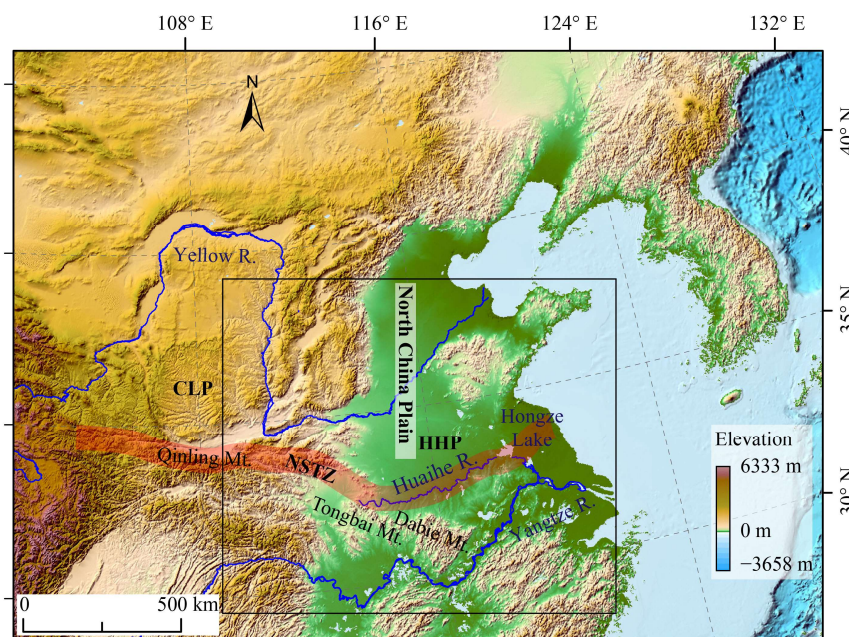


Figure 1. Location of the HHR. The figure shows the topography of the study area and its surroundings. HHP: Huanghuai Plain; CLP: Chinese Loess Plateau; NSTZ: China’s North–South Transitional Zone. The rectangular box indicates the location of Figure 2a.

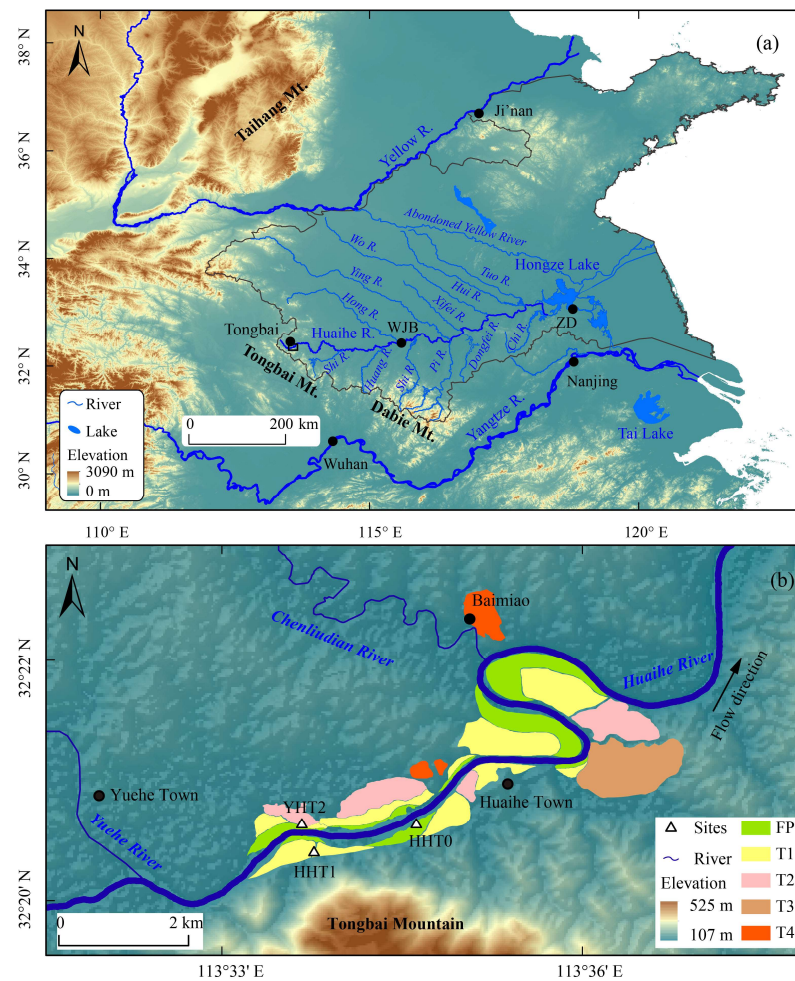


Figure 2. (a) River systems of the HHR Basin; (b) Distribution of the HHR terraces and location of our studied outcrops. WJB: Wangjiaba. ZD: Zhongdu. FP: Floodplain. The rectangular box in Figure 2a indicates the location of Figure 2b.

2. Study Area

2.1. Geographic Settings

The HHR Basin lies in the southern sector of the North China Plain (NCP) (Figure 1). There are various landforms within the basin, but it is dominated by plains (i.e., the Huanghuai Plain), platforms, and depressions, accounting for ~83% of the basin's total area, with the remainder of the land surface being composed of low mountains and hills [29]. The HHR originates in the Tongbai Mountains in southwestern Henan Province. The Tongbai Mountains area is located in the southwest of the HHR Basin. The main stream of the HHR can be divided into its upper reaches from its source to Wangjiaba, its middle reaches from Wangjiaba to Zhongdu, near Lake Hongze, and its lower reaches below Zhongdu (Figure 2a). The main stream of the HHR, with a length of 1000 km, flows along the northern flanks of the Tongbai–Dabie orogenic belt. The river system of the HHR Basin is significantly affected by regional topography, and the direction of flow of tributaries on both sides of the HHR is consistent with the topography (Figure 2a). In addition, the tributaries on the northern side of the trunk mostly have longer river lengths and a lower mean channel gradient than the tributaries on the HHR's southern side. The gradient of the HHR's main channel is 0.2‰, with a mean value of 0.5‰ in its upper reaches. This gentle gradient results in a poor flood-retention capacity and a wandering channel [30].

The precipitation is mainly concentrated in summer and supplies 55–80% of the mean annual precipitation (MAP) of the HHR Basin [29]. The mean annual temperature (MAT) and MAP of the HHR Basin are 13–16 °C and 883 mm, respectively. The MAP

varies from 600–1400 mm, with the highest value of 1400 mm falling in the Tongbai–Dabie mountain area.

2.2. Paleoclimates

Abundant evidence has suggested that significant climatic fluctuations occurred in the HHR Basin during the Late Quaternary [31–35]. A summary of Late Quaternary paleoclimates in the HHR Basin is detailed below and summarized in Table 1.

In the upper HHR Basin, based on analyses of the sporo-pollens, micropaleontologic evidence and geochemical elements within the Huzupu Profile in Xinyang Prefecture in southernmost Henan Province, it has been suggested that during 30–25 ka, the area covered by lakes experienced multiple periods of expansion and contraction, potentially reflecting abnormal climatic fluctuations during the Marine Isotope Stage (MIS) 3/2 transition. From 25 to 13 ka, the regional climate experienced a change from warm–wet to warm–dry, and then to warm–wet [33]. Additionally, there was a relatively humid climate from 40 to 30 ka, and a relatively dry and cold climate during 30–18.6 ka in the lower HHR Basin [36]. Moreover, studies of the lacustrine deposits found in the Shagou Core have indicated that there were climatic fluctuations during MIS 2, such as a relatively humid stage during 30–26 ka, a drying stage between 26 and 18 ka, and a relatively warm and wet stage throughout 18–15 ka [37].

During the Holocene, the climate of the study area was similar to that indicative of the East Asian Monsoon (EAM) area [38–40]. The stalagmite record from Magou Cave shows that monsoonal precipitation in the region gradually increased from 11.2 to 9.1 ka and maintained a relatively high value from 9.1 to 4.9 ka [41]. In addition, the clay content of the Yuzhou loess record gradually increased from 11.5 to 8.5 ka, reaching its maximum at 8.5–3.1 ka before decreasing after 3.1 ka [32]. However, the clay content of the Yuzhou profile increased again after 1.5 ka [32], potentially indicating that there was a certain humidifying trend after 1.5 ka. Historical documents for the past 1,000 yr indicate that the Medieval Climate Anomaly (MCA) that occurred in the Jiang–Huai area (east of 105° E; ~31–34° N) was warm and dry, while the Little Ice Age (LIA) was cold and wet [42–44].

Moreover, the Xiangcheng loess sequence from the upper HHR Basin suggests that there was a different climatic regime during the Late Holocene. It indicates that the warmest and most humid period here occurred at 3.8–1.8 ka [45]. In addition, the lacustrine records from the lower HHR Basin indicate a relatively warm and humid Late Holocene period [46,47]. This difference in climate between the upper and lower HHR Basin might reflect the influence of local natural factors on the local climate [34,48–50].

Table 1. Summary of climate changes in the HHR Basin during the Quaternary.

MIS	Upper HHR Basin	Middle HHR Basin		Lower HHR Basin		
	Huzupu [33]	Xiangcheng [45]	Yuzhou [32]	Yinzhuangqiao [47]	Zhoufen [36]	Shagou [37]
1	Warm–wet (since 13 ka)	Cold–wet to warm–dry (since 1.8 ka) Warm–wet (3.8–1.8 ka) Cold–dry (4.5–3.8 ka) Cold–wet (5.8–4.5 ka) Warm to cold–dry (12.1–5.8 ka)	Cold–dry (since 3.1 ka) Warm–wet (8.5–3.1 ka) Warming and wetting (11.5–8.5 ka)	Warm–wet (5–1.5 ka) Cooling and drying (7.5–5 ka) Warm–wet (11.3–7.5 ka)		
2	Warm–dry to warm–wet (25–13 ka) Warm–wet (30–25 ka)			Cold–dry (13–11.3 ka) Warm–wet (14.2–13 ka) Cold–dry (19.2–14.2 ka)	Cold–dry (30–18.6 ka)	Warm–wet (18–15 ka) Dry (26–18 ka) Wet (30–26 ka)
3					Wet (40–30 ka)	

3. Sampling and Methodology

3.1. Fieldwork

At least four river terraces were found to have developed in the upper HHR near the Tongbai Mountains (Figures 2b and 3). Terraces T4 and T3 are located in the Huaihe Town area. The floodplain (FP), Terraces T1 and T2 are well-developed along both flanks of the upper HHR. We conducted field observations of the lower three geomorphic surfaces (i.e., FP, Terraces T2 and T1). In this study, we chose three outcrops (YHT2, HHT1, and HHT0) for investigation (Figure 3). Sedimentary architectures were delineated and described in the field. Samples were then taken for laboratory analysis.

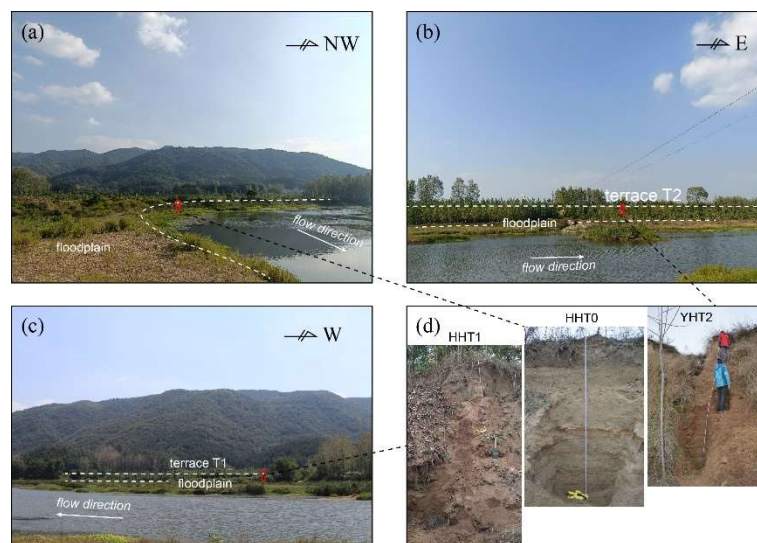


Figure 3. Field photos of the floodplain (a), Terraces T2 (b) and T1 (c), and studied outcrops (d).

3.2. Grain Size

Samples for grain size analysis were collected at 5 cm intervals over the three outcrops. The samples were both treated and measured in the Key Laboratory of Western China's Environmental Systems (Ministry of Education) at Lanzhou University. In the laboratory, grain size samples were first treated with HCl and H₂O₂ to remove carbonates and organic matter, respectively. Then, the purified samples were measured using a Malvern Mastersizer 2000 (Malvern Instruments Ltd., Worcestershire, UK) laser particle sizer.

3.3. Dating Methods

Charcoal and organic sediments were sampled for ¹⁴C dating. These materials were both pretreated and measured at the Beta Analytic Radiocarbon Laboratory. The ¹⁴C dates were calibrated using BetaCal3.21 software and the Northern Hemisphere atmospheric ¹⁴C calibration dataset IntCal13 [51]. The AMS dating results are listed in Table 2.

Table 2. AMS and conventional radiocarbon dates from HHT1 and HHT0 outcrops.

Laboratory Code	Outcrop	Depth (m)	Dated Material	$\delta^{13}\text{C}$ (‰)	¹⁴ C Age (a BP)	Calibrated ¹⁴ C Age (cal. a BP)
Beta-546613	HHT0	1.46	Charcoal	−26.3	210 ± 30	216–144
Beta-546614	HHT0	1.35	Charcoal	−26.0	160 ± 30	231–124
Beta-546617	HHT1	4.70	Organic sediment	−22.6	3000 ± 30	3253–3075

The OSL samples were collected from freshly cleaned sections using steel tubes. All laboratory analyses were conducted in the luminescence laboratory at the Qinghai

Institute of Salt Lakes. The unexposed central section of each sample was used for OSL measurements to estimate the equivalent dose (D_e). The samples were treated with 10% HCl and 30% H₂O₂ to remove carbonates and organic matter, respectively. Coarse silt fraction (38–63 μm) of these samples was wet sieved and etched with 35% hydrofluorosilicic acid (H₂SiF₆) for two weeks to remove feldspars. Finally, 10% HCl was used to remove fluoride precipitates [52,53].

OSL signals were measured using a Risø TL/OSL-DA-20 reader. D_e was determined using a combination of the single-aliquot regenerative-dose (SAR) protocol [54] and the standardized growth curve (SGC) method [55–57]. Environmental dose rates were calculated based on Prescott and Hutton [58] and the contents of U, Th, and K.

A preheat plateau test was conducted for samples ISL-Lum-2020-515 and ISL-Lum-2020-32 (Figure 4). A plateau was observed for temperatures ranging from 240 to 260 °C for both samples. Recuperation for the 200-to-300 °C preheat temperatures was <1% of the natural signal (Figure 4a). The recycling ratios for different preheat temperatures all fell into a range of 0.9–1.1 (Figure 4b). Therefore, the SAR protocol with a preheat temperature of 260 °C and a second preheat of 220 °C after test dose was selected to measure the D_e . The OSL decay and growth curves for samples ISL-Lum-2020-515 and ISL-Lum-2020-32 are shown in Figure 5. The blue light-stimulated OSL signals decreased very quickly during the first second of stimulation, indicating that the signal is dominated by the fast component [59]. The OSL results are listed in Tables 3 and 4.

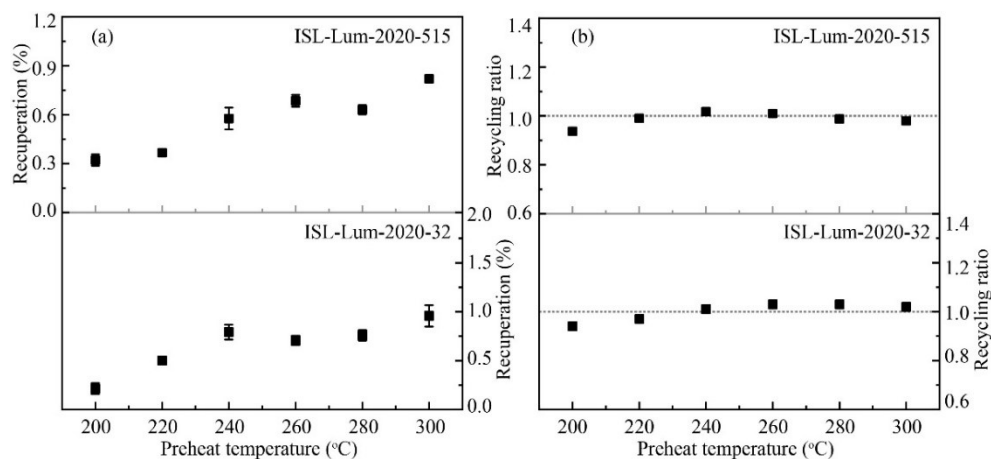


Figure 4. Preheat plateau test of the OSL signal on temperature for samples ISL-Lum-2020-515 and ISL-Lum-2020-32. The figure shows the dependence of recuperation (a) and recycling ratio (b) on preheat temperature.

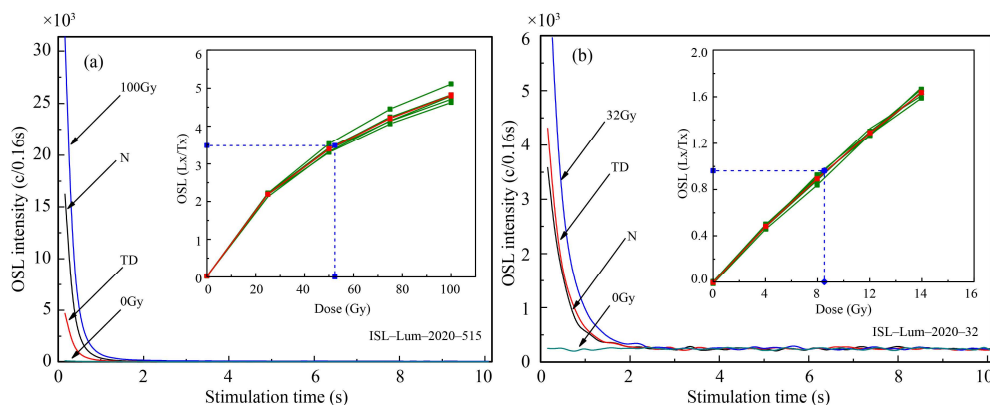


Figure 5. Typical OSL decay curves and growth curves (insert) of samples ISL-Lum-2020-515 (a) and ISL-Lum-2020-32 (b).

Table 3. OSL dating results for samples taken from YHT2 outcrop.

Laboratory Code	Outcrop	Depth (m)	Grain (μm)	K (%)	Th (ppm)	U (ppm)	Water Content (%)	Dose Rate(Gy/ka)	De (Gy)	OSL Age (ka)
ISL-Lum-2020-524	YHT2	0.4	38–63	1.96 ± 0.04	12.84 ± 0.70	2.22 ± 0.30	21 ± 5	2.98 ± 0.22	17.2 ± 0.3	5.8 ± 0.4
ISL-Lum-2020-523	YHT2	2.0	38–63	2.03 ± 0.04	11.76 ± 0.70	2.11 ± 0.30	18 ± 5	3.02 ± 0.22	53.2 ± 1.6	17.6 ± 1.4
ISL-Lum-2020-521	YHT2	4.1	38–63	1.94 ± 0.04	11.58 ± 0.70	2.00 ± 0.30	20 ± 5	2.82 ± 0.21	53.2 ± 1.1	18.9 ± 1.5
ISL-Lum-2020-519	YHT2	5.0	38–63	1.83 ± 0.04	10.27 ± 0.70	1.70 ± 0.30	14 ± 5	2.77 ± 0.21	54.6 ± 1.2	19.7 ± 1.6
ISL-Lum-2020-518	YHT2	5.4	38–63	1.82 ± 0.04	10.44 ± 0.70	1.82 ± 0.30	25 ± 5	2.40 ± 0.19	51.6 ± 1.0	21.5 ± 1.7
ISL-Lum-2020-517	YHT2	5.6	38–63	1.54 ± 0.04	6.88 ± 0.60	1.29 ± 0.30	16 ± 5	2.12 ± 0.17	51.8 ± 1.7	24.4 ± 2.1
ISL-Lum-2020-516	YHT2	5.8	38–63	1.83 ± 0.04	9.06 ± 0.60	1.62 ± 0.30	13 ± 5	2.71 ± 0.21	49.5 ± 1.3	18.3 ± 1.5
ISL-Lum-2020-515	YHT2	6.1	38–63	1.74 ± 0.04	6.63 ± 0.60	1.29 ± 0.30	16 ± 5	2.27 ± 0.18	53.2 ± 1.8	23.4 ± 2.1

Table 4. OSL dating results for samples taken from HHT1 outcrop.

Laboratory Code	Outcrop	Depth (m)	Grain (μm)	K (%)	Th (ppm)	U (ppm)	Water Content (%)	Dose Rate (Gy/ka)	De (Gy)	OSL Age (ka)
ISL-Lum-2020-35	HHT1	0.55	38–63	2.41 ± 0.04	12.30 ± 0.70	2.98 ± 0.40	15 ± 5	4.02 ± 0.29	2.1 ± 0.6	0.5 ± 0.2
ISL-Lum-2020-34	HHT1	1.60	38–63	1.87 ± 0.04	10.27 ± 0.70	2.14 ± 0.30	15 ± 5	3.31 ± 0.25	5.9 ± 0.3	1.8 ± 0.2
ISL-Lum-2020-33	HHT1	3.30	38–63	1.42 ± 0.04	8.91 ± 0.60	1.86 ± 0.30	15 ± 5	2.50 ± 0.19	7.8 ± 0.1	3.1 ± 0.2
ISL-Lum-2020-32	HHT1	4.35	38–63	1.28 ± 0.04	7.23 ± 0.60	1.40 ± 0.20	15 ± 5	1.96 ± 0.15	9.1 ± 0.3	4.6 ± 0.4
ISL-Lum-2020-31	HHT1	4.60	38–63	2.00 ± 0.04	13.80 ± 0.80	1.52 ± 0.30	15 ± 5	3.04 ± 0.23	10.1 ± 0.3	3.3 ± 0.3

4. Results

4.1. Stratigraphy

4.1.1. YHT2 Outcrop

The YHT2 outcrop lies on the northern flank of the HHR near Yuehe Town (Figures 2b and 3). The uppermost surface of this outcrop is ~9.1 m above the modern river level (arl). The upper 6.4 m of this profile were studied. Six sedimentary units were identified (Figure 6).

The lowermost unit (U1; 6.4–6.2 m) is composed of reddish-brown medium sands, which were interpreted as channel-fill deposits. Unit U2 (6.2–5.58 m) was divided into three subunits (U2a, U2b, and U2c). The lower subunit (U2a; 6.2–6.1m) is composed of blue-gray fine sands interbedded with thin layers of yellow-brown fine sands. The subunit U2b (6.1–5.74 m) consists of yellow-gray fine sands with parallel bedding, but the lower part of U2b is interbedded with some layers of blue-gray fine sands. The upper subunit (U2c; 5.74–5.58 m) is dominated by blue-gray fine sands and silts. There are some thin layers of yellow-gray fine sands that were identified in the lower part of U2c. This interbedding of blue-gray and yellow-gray fine sands might indicate transformations between fluvial (sandbar) and backswamp environments. Unit U3 (5.58–5.4 m) consists of yellow-gray fine sands with parallel bedding, which indicates sheet-flood deposits on the top of the sand bar. Unit U4 (5.4–4.1 m) consists of yellow-gray silts, with few layers of fine sands. The composition of this unit implies the existence of a relatively stable environment, during which time a floodplain developed. Unit U5 (4.1–0.4 m) is dominated by silts. This unit can be subdivided into two parts. The lower part (U5a; 4.1–0.7 m) is composed of reddish-brown silts. It is dense and massive, containing many gray-white stripes and rusty brown mottles, potentially the result of strong leaching. In addition, the upper part (U5b; 0.7–0.4 m) is composed of yellow-gray silts with many reddish-brown rusty spots, implying strong leaching and deposition. The uppermost unit (U6), at 0.4–0 m, has been influenced by modern human activity and contains many

plant roots. The backswamp deposits at the bottom of U2, and the thick layer of overbank deposits at Units U4 and U5, may indicate the development of floodplains in a meandering or anastomosing river system. However, lacustrine deposits and coal commonly occur in association with anastomosing river overbank deposits in humid areas [60,61]. Therefore, based on this sedimentary structure and lithofacies models [62], we deduced that the YHT2 section indicates a meandering channel system.

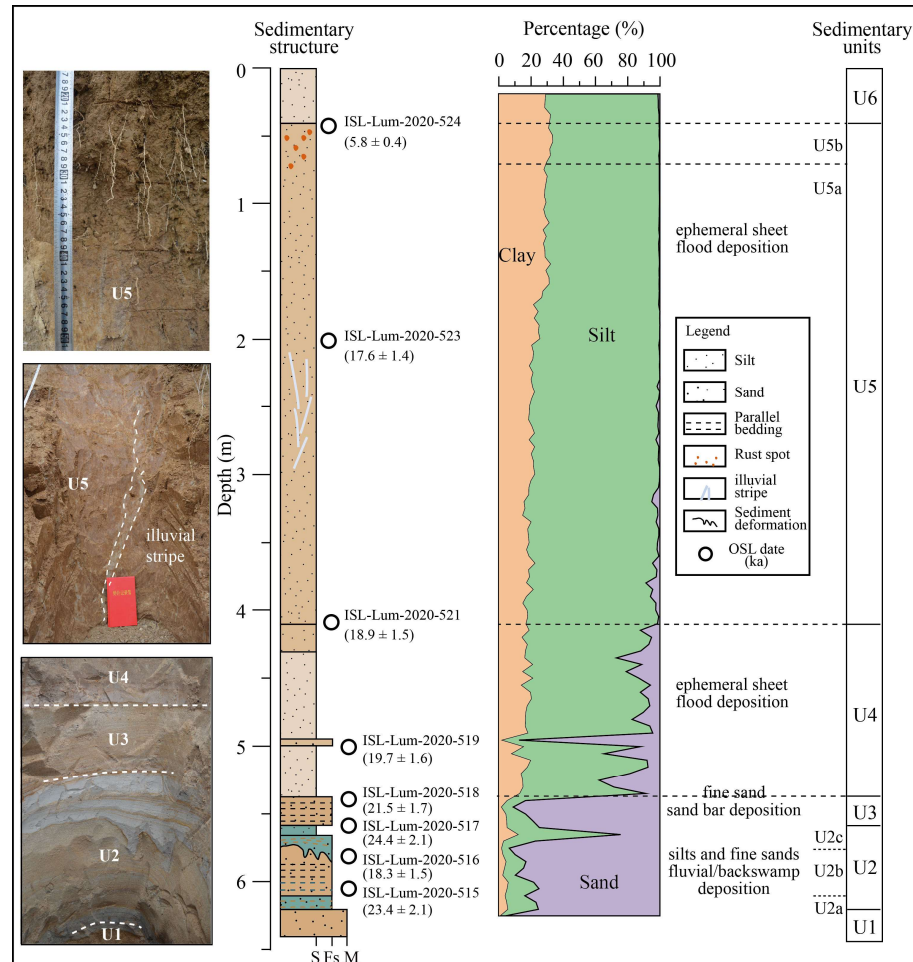


Figure 6. Field photos and sedimentary architecture of the YHT2 outcrop. S: silt; Fs: fine sand; M: medium sand.

4.1.2. HHT1 Outcrop

The HHT1 outcrop is located on the southern flank of the HHR near Huaihe Town. The top of this terrace is about 6 m arl. Six sedimentary units were identified (Figure 7).

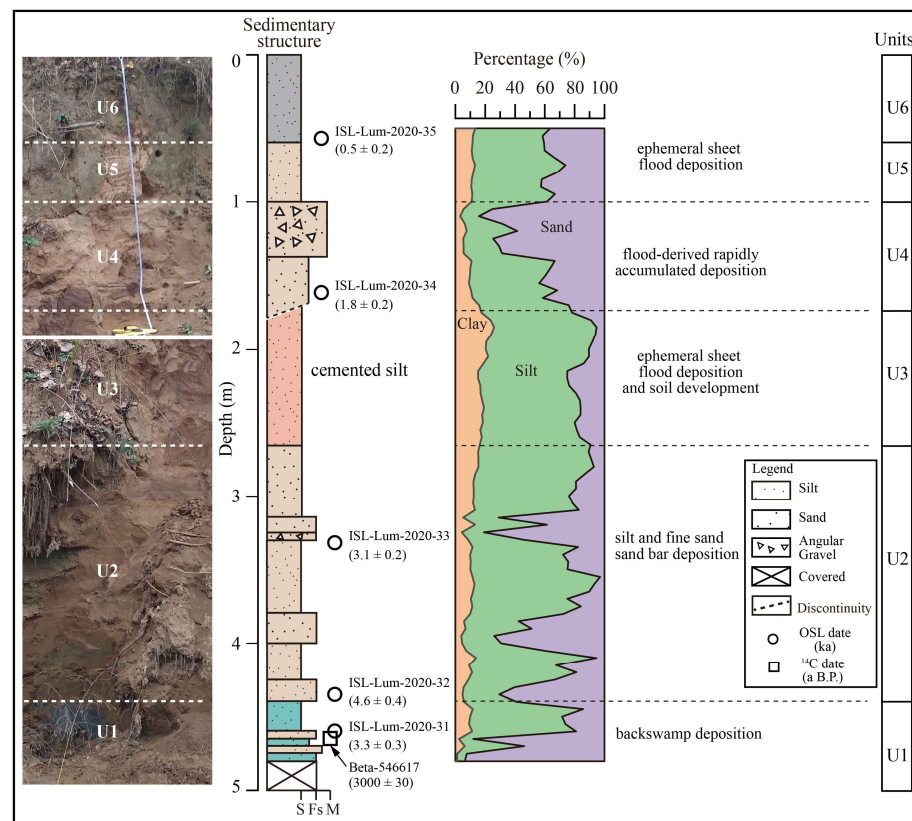


Figure 7. Field photos and sedimentary characteristics of the HHT1 outcrop. S: silt; Fs: fine sand; M: medium sand.

The lowermost unit (U1; 4.8–4.41 m) consists of blue-gray silts and fine sands. Two layers of yellow-gray fine sands were observed in this unit. The composition of U1 might indicate backswamp deposits, interrupted by channel bedloads. U2 lies between 4.41 and 2.65 m and is composed of yellow-gray fluvial silts and fine sands. There are some rust-colored spots, but no sedimentary structures were clearly identified. Some angular gravels with a grain size of 3–5 cm were observed between 3.30–3.25 m. The composition of U2 might indicate the development of a sand bar in the main river channel. U3 (2.65–1.70 m) is characterized by reddish-brown, colloidal, clayey silts, with a dense and massive structure; this can be attributed to ephemeral sheet flood deposits accumulated during floodplain development. U4 (1.7–1.0 m) is in unconformable contact with the underlying U3. An inclined sedimentary discontinuity was observed at the base of U4, potentially implying an erosion event. In addition, the lower part of U4 consists of yellow-gray silts and fine sands; its upper part is composed of fine-to-medium sands, with some angular gravels. The composition of this unit might indicate a rapid accumulation process. U5 (1.0–0.6 m) is composed of yellow-gray silts. The uppermost unit (U6), at 0.6–0 m, is affected by plant development and has a grayish-black color. U5 and U6 represent floodplain deposits accumulated under gentle hydrodynamic conditions. Based on the composition of this sedimentary structure and lithofacies models [62], we deduced that the HHT1 profile indicates a meandering river environment, including a period when backswamp deposits developed.

4.1.3. HHT0 Outcrop

The HHT0 outcrop, located on the southern flank of the HHR near Huaihe Town, is the modern floodplain (Figure 3). The top surface of this profile is ~4 m a.r.l. Only the upper 2 m of this profile was studied (Figure 8). It was divided into six sedimentary units.

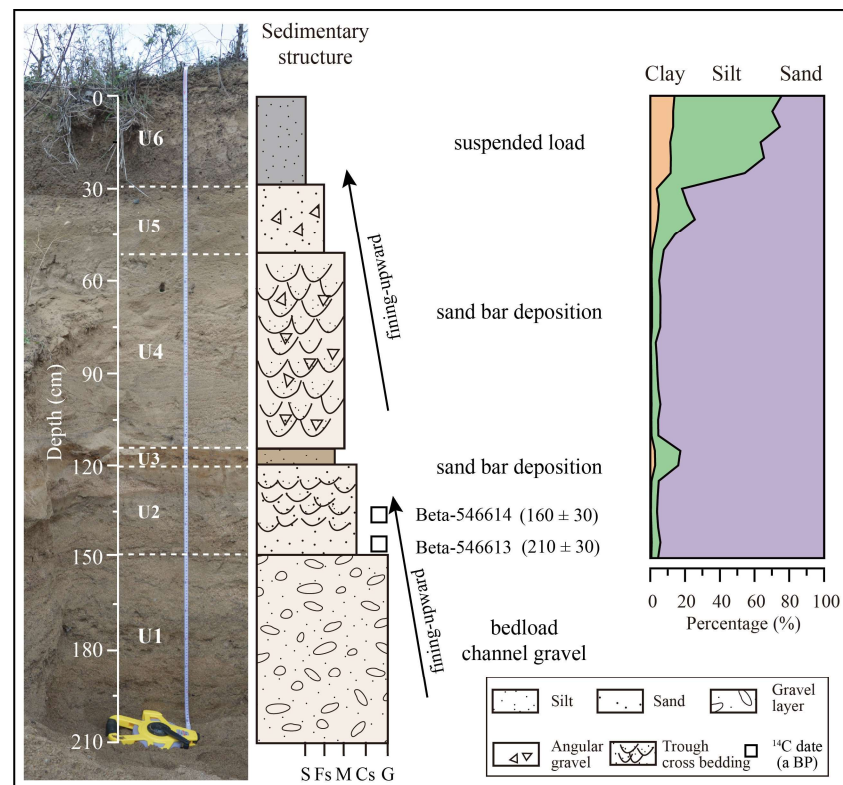


Figure 8. Field photos and sedimentary architecture of the HHT0 outcrop. S: silt; Fs: fine sand; M: medium sand; Cs: coarse sand; G: gravel.

The lowermost unit (U1) occurs between 2.1 and 1.5 m below the surface and is dominated by gravels and coarse-grained sands. The unit U2 (1.5–1.2 m) is characterized by medium-to-coarse sands, with small-scale (5–10 cm thick, ~10 cm width) trough cross-bedding. The upper unit U3 (1.2–1.14 m) is composed of a layer of brown fine-to-medium sands. We therefore deduced that U2 and U3 might indicate sand bar deposits. U4 (1.14–0.5 m) is dominated by yellow-gray medium sands, interbedded with thin layers of angular gravels. Small-scale (10–15 cm thick and 10–30 cm width) trough cross-bedding was observed in U4. The unit U5 (0.5–0.29 m) consists of fine sands, with few angular gravels observed. The units U4 and U5 were attributed to the lower parts of point-bar deposits. The uppermost unit (U6; 0.29–0 m) is composed of black-gray silts affected by surface vegetation. Therefore, U6 was attributed to sheet-flood deposits. As a part of the modern HHR floodplain, this sedimentary profile indicates a sedimentary assemblage typical of modern wandering channels.

4.2. Dating Results

The AMS and OSL dating yielded 16 age results ranging from 24.4 to 0.16 ka (Tables 1–3). In the bottom of the YHT2 outcrop, three OSL ages in unit U2 were dated around 24.4–18.3 ka (Figure 6), indicating that the onset of accumulation in this profile might have started around the Last Glacial Maximum (LGM). The sample ISL–Lum–2020–516 in the middle part of U2 was dated at 18.3 ka, which is younger than the above three ages in units U3 and U4, although it might be underestimated. In addition, one age (ISL–Lum–2020–524, 5.8 ka) was obtained in Unit U6 at the top of the profile, indicating that the end of accumulation occurred around 5.8 ka. In the HHT1 outcrop, an OSL age (ISL–Lum–2020–31, 3.3 ka) and AMS age (Beta–546617, 3000 a B.P.) were obtained in U1, indicating that the HHT1 aggraded around 3 ka (Figure 7). However, an older age of 4.6 ka (ISL–Lum–2020–32) was dated in the upper unit U2. Thus, it was regarded as an outlier. An age of 0.5 ka (ISL–Lum–2020–35) was obtained in U6, indicating the end of deposition of the HHT1 profile. In the HHT0 outcrop, two AMS ages

(Beta-546613, Beta-546614) at the top of unit U1 were dated at 210–160 a B.P., indicating that the accumulation of modern floodplains might take place around 0.2 ka. All dating results are generally consistent with the internal stratigraphical positions, except for the overestimated sample ISL-Lum-2020-32 in HHT1 and underestimated sample ISL-Lum-2020-516 in YHT2.

5. Discussion

5.1. Late Quaternary Fluvial Processes in the Upper HHR

Using our sedimentary analyses and dating of the three profiles (YHT2, HHT1, and HHT0), we reconstructed the fluvial processes of the upper HHR near Tongbai since the LGM (Figure 9). From the LGM to 5.8 ka, the upper HHR was dominated by an aggrading, meandering channel. The gray-white stripes and rusty-brown mottles within the sedimentary profile (YHT2; Figure 6) would indicate strong leaching and soil development during the formation of the floodplain. However, a period characterized by transformations between sandbar and backswamp deposits was identified as having occurred during the LGM (Figure 6). Subsequently, a channel incision/erosion event occurred at 5.8–3 ka (Figure 9). At ~3 ka, another period of transformations between fluvial and backswamp deposits took place (Figure 7). After that, from 3 to 0.5 ka, a meandering channel developed in the study area. However, a marked erosion event took place at ~1.8 ka, identified by a discontinuity in the HHT1 profile. In addition, river downcutting occurred at 0.5–0.2 ka, followed by the development of the modern wandering channel (Figure 9).

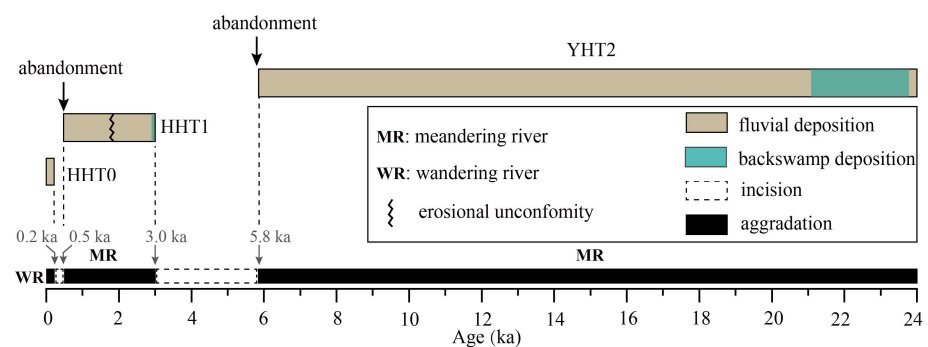


Figure 9. Schematic diagram of fluvial processes in the upper HHR.

5.2. Fluvial Responses to Climate Change in the Upper HHR

Climate change can regulate river behaviors, i.e., via aggradation/incision processes and changes to channel patterns, by affecting runoff, vegetation, and soil cohesion [4,5,11,17,63]. The downcutting events observed in the upper HHR show a clear correlation with regional climate change (Figure 10). For example, the channel incision that occurred at 5.8–3 ka was likely triggered by climate change during the Mid-Late Holocene transition. During this transition period, the regional climate became increasingly unstable, as indicated by loess (Figure 10d) [45] and peat records (Figure 10e) [64]. Moreover, there is evidence that there was a relatively warm, humid, and increasingly unstable climate in the HHR Basin during this transition period [31,32,45,46]. For example, the grain size of fine particles (1–5 μm) in the Yuzhou loess profile increases until it eventually reaches its largest value during the Holocene (Figure 10a) [32]. The decrease in the magnetic susceptibility of the Yinzhuangqiao profile in northern Jiangsu Province also indicates a similar warm-wet but transitional climatic regime (Figure 10b) [47]. We can therefore deduce that the channel incision in the upper reaches of the HHR might have been the result of increasingly heavy seasonal precipitation triggered by a climatic transition within the context of a warm, humid climatic background.

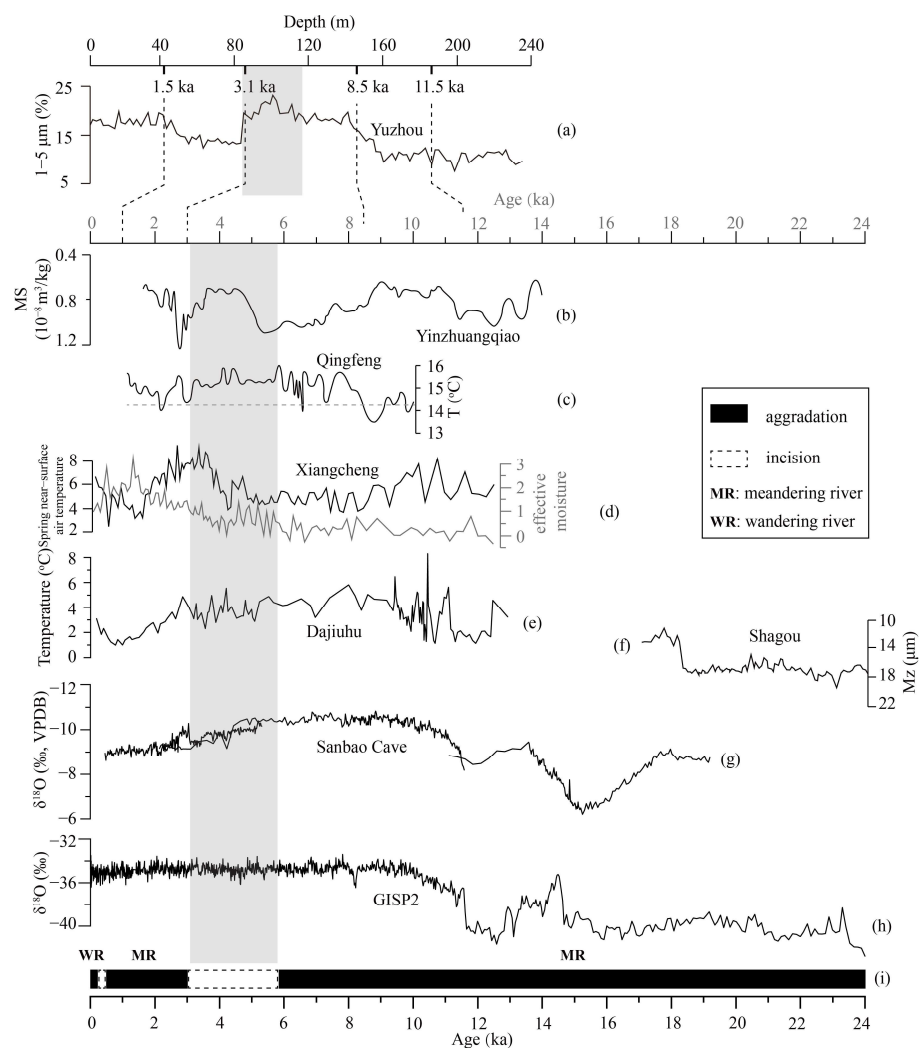


Figure 10. Correlation of the fluvial processes and changes in climate in the upper HHR since the LGM. (a) The content of fine materials in the Yuzhou loess profile in Yuzhou [32]; (b) magnetic susceptibility of the Yin Zhuangqiao Core [47]; (c) reconstructed Holocene temperature of the Qingfeng Profile [31]; (d) reconstructed temperature and moisture for the Xiangcheng Profile [45]; (e) reconstructed temperature of the Dajiuhe Core [64]; (f) mean grain size of the Shagou Core [37]; (g) stalagmite $\delta^{18}\text{O}$ data from Sanbao Cave [40]; (h) oxygen isotope record of the GISP2 ice core in Greenland [38]; and (i) schematic diagram of fluvial processes of the upper HHR.

Additionally, the downcutting that occurred at 0.5–0.2 ka might be driven by regional climate change during the LIA (Figure 11). It has been suggested, based on sedimentary and literary climate records, that there was a relatively warm and dry MCA, but a cold and wet LIA in the Jiang–Huai area (Figure 11a,b) [42–44,65,66]. Moreover, meteorological disaster reconstructions, based on the literature, have indicated that there was a significant increase in extreme flood events during the LIA (Figure 11c) [67]. Therefore, we deduced that frequent high-amplitude floods during the LIA forced the river incision observed in the upper HHR.

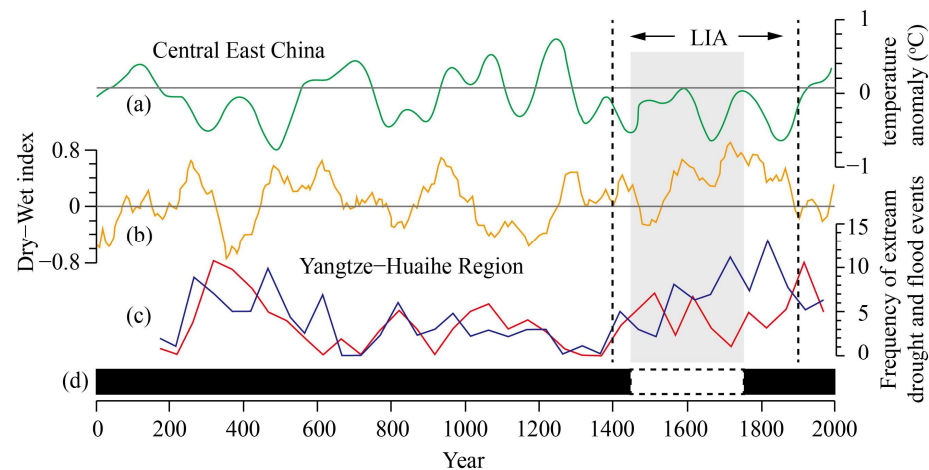


Figure 11. Changes in climate and fluvial processes in the upper HHR during the past 2000 years. (a) The upper green curve indicates a temperature anomaly in the central eastern China [65]; (b) the middle-orange curve indicates a dry-wet index derived from historical documents from the Jiang–Huai area, eastern China [66]; (c) the lower-blue and red curves indicate extreme flood and drought events, respectively, in the Jiang–Huai area [67]; and (d) the fluvial processes of the upper HHR over the past 2000 years. The black section indicates aggradation; the dotted-white section indicates river incision.

Numerous studies have suggested that there was a cold and drying climate during the LGM [33,36,37] in the HHR Basin, as well as an amelioration of the regional hydroclimate since the last deglaciation [34,35]. Recently, a quantitative study based on pollen records has indicated that during the LGM in China, the MAT was $\sim 5.6 \pm 0.8$ °C lower than today's, while the MAP was $\sim 46.3 \pm 17.8$ mm lower [68]. Moreover, the MAP fell further in northern China (by $\sim 51.2 \pm 21.4$ mm), whereas a small decrease of $\sim 0.2 \pm 41.5$ mm occurred in southern China [68]. In addition, vegetation reconstructions of the NCP have indicated that regional vegetation patterns in the north changed from grassland to forest, and that, while forest was always present in the south, this region was characterized by a clear change in vegetation type after the LGM [69]. Therefore, there was no clear climatic deterioration in the study area during the LGM, but there was a relatively colder, wet climate. The meandering channel pattern with no marked changes observed in the study area would, therefore, suggest forest vegetation and a wet climate during the LGM.

Additionally, several layers of blue-gray, backswamp deposits developed at ~ 3 ka during the LGM. This backswamp deposition points to an overwetting environment on the floodplain and sandbar caused by frequent flooding. The transformations between fluvial and backswamp deposits during these two periods, therefore, indicate the presence of a relatively wet and transitional climatic regime.

5.3. Regional Differentiation

Although climate change can significantly affect river behavior, fluvial responses to climate change often exhibit significant complexity due to the effects of local topography, vegetation, and internal adjustments within river systems [1,4,17,19,26]. Our results showed that the upper HHR were incised during the Mid–Late Holocene transition (5.8–3 ka), a phenomenon also observed in other rivers in Northwestern China [17,70]. Moreover, the undercutting of rivers in this period can be compared to other river courses on a global scale, e.g., the Cowhouse Creek in the USA [71] and many rivers in Europe [72,73]. However, not all climatic transitions are known to have driven river incision. For example, the upper HHR was still dominated by aggradation towards the end of the LGM, as well as the last deglaciation–Holocene transition. Such non-linear fluvial responses to climate change, potentially related to internal adjustments within individual river systems, have also been noted in other regions [17,74,75].

Additionally, there have been no marked changes in channel patterns in the upper HHR since the LGM. However, in contrast, the Shiyang River in arid northwestern China was characterized by a braided channel during the 22–13 ka period and a meandering channel between 13 and 5 ka [17]. Furthermore, changes in river channel patterns at the end of the LGM appear to have been widespread in other regions, such as in humid/semi-humid areas of Europe (once influenced by glacial/periglacial processes) [76–78] and the humid subtropical regions of the USA (not influenced by glacial/periglacial landscapes) [79]. The uniqueness of the upper HHR might, therefore, represent the impact of local climatic and vegetation controls. The wet climate and forest-dominated vegetation prevalent in the region since the LGM might be the main reason for the unchanged river channel patterns observed in the upper HHR. Similarly, the reconstructed Last Glacial fluvial history in the Netherlands showed that the effects of climate change on river systems depend mainly on changes in vegetation [76].

On a broader, global scale, it may be deduced that the differences evident in river behavior in different regions may be caused by local hydroclimatic regimes. For example, on the Gujarat Plain in arid areas of Northwestern India, there is evidence of an active, meandering channel during MIS 3 but an aeolian-dominated phase during MIS 2, as well as transformations between fluvial and aeolian processes during the Holocene [26]. Significant differences between fluvial processes also existed in Central and Southeastern Australia during the LGM and Late Glacial. During these periods, arid Central Australia experienced a break in river activity, whilst humid Southeastern Australia remained fluvially active [80]. Furthermore, three geosystem types developed in Western Peru during the Holocene under the influence of local topographic and hydroclimatic conditions: coastal desert; lomas (with tafone widely developed); and mountain desert (with active fluvial activities during El Niño events) [18].

The above analysis also revealed that regional geomorphic processes are manifested differently in different climatic zones. In humid zones, climate-driven fluvial processes can be the dominant factors in regional geomorphologic evolution in humid areas. In arid and semi-arid areas, aeolian processes can be superimposed on river processes, and climate-influenced aeolian–fluvial interactions become the main factor controlling regional geomorphic processes [19,26,63,81]. In addition, in glacial or periglacial areas, changes in glacier advance and retreat, vegetation cover, and seasonal permafrost due to climate fluctuations can combine to influence surface runoff and sediment yield, and glacial–fluvial–lacustrine processes may dominate regional geomorphic processes [5,23,82].

6. Conclusions

This work provides a case study of fluvial processes in a unique humid region (China's NSTZ) and evaluates the influence of the local hydroclimate on the upper HHR. River downcutting occurred mainly during the Mid–Late Holocene transition and the LIA, potentially as the result of floods triggered by climate change. In addition, the river's channel pattern has not changed significantly since LGM. The study area has not experienced significant aridity and vegetation change since the LGM, explaining the relatively stable channel pattern observed in the area. More broadly, significant differences in fluvial processes occurring under different climatic–geomorphic conditions were found. Changes in the local hydroclimatic regime might be the most important factor driving these dissimilarities. Future research into fluvial processes in different geomorphologic–climatic regions is now required to comprehend more clearly the relationships between rivers and local hydroclimatic factors.

Author Contributions: Conceptualization, Z.L., H.G. and Y.W.; formal analysis, W.Z. and W.X.; investigation, F.L., C.Z. and W.X.; visualization, W.Z., X.L. and Q.Q.; writing—original draft preparation, Z.L. and Y.W.; writing—review and editing, Z.L. and Y.W. All authors have read and agreed to the published version of the manuscript.

Funding: This work was supported by the National Natural Science Foundation of China (Grant No. 41901007), and the Nanhu Scholars' Program for Young Scholars of XYNU.

Data Availability Statement: Not applicable.

Conflicts of Interest: The authors declare no conflict of interest.

References

1. Bull, W.B. *Geomorphic Responses to Climatic Change*; Oxford University Press: New York, NY, USA, 1991.
2. Pan, B.T.; Su, H.; Hu, Z.B.; Hu, X.F.; Gao, H.S.; Li, J.J.; Kirby, E. Evaluating the role of climate and tectonics during non-steady incision of the Yellow River: Evidence from a 1.24 Ma terrace record near Lanzhou, China. *Quat. Sci. Rev.* **2009**, *28*, 3281–3290. [[CrossRef](#)]
3. Bridgland, D.R.; Westaway, R. Quaternary fluvial archives and landscape evolution: A global synthesis. *Proc. Geol. Assoc.* **2014**, *125*, 600–629. [[CrossRef](#)]
4. Vandenberghe, J. River terraces as a response to climatic forcing: Formation processes, sedimentary characteristics and sites for human occupation. *Quat. Int.* **2015**, *370*, 3–11. [[CrossRef](#)]
5. Cordier, S.; Adamson, K.; Delmas, M.; Calvet, M.; Harmand, D. Of ice and water: Quaternary fluvial response to glacial forcing. *Quat. Sci. Rev.* **2017**, *166*, 57–73. [[CrossRef](#)]
6. Gao, H.S.; Li, Z.M.; Liu, F.L.; Wu, Y.J.; Li, P.; Zhao, X.; Li, F.Q.; Guo, J.; Liu, C.R.; Pan, B.T.; et al. Terrace formation and river valley development along the lower Taohe River in central China. *Geomorphology* **2020**, *348*, 106885. [[CrossRef](#)]
7. Maddy, D.; Veldkamp, A.; Demir, T.; Aytac, A.S.; Schoorl, J.M.; Scaife, R.; Boomer, I.; Stemerink, C.; van der Schriek, T.; Aksay, S.; et al. Early Pleistocene River Terraces of the Gediz River, Turkey: The role of faulting, fracturing, volcanism and travertines in their genesis. *Geomorphology* **2020**, *358*, 107102. [[CrossRef](#)]
8. Vandenberghe, J.; Yang, X.; Wang, X.Y.; Wang, S.J.; Lu, H.Y. Diverse floodplain deposits of reworked loess in a monsoon climate (Hanzhong Basin, central China). *Quat. Res.* **2021**, *103*, 4–20. [[CrossRef](#)]
9. Yu, Y.; Wang, X.Y.; Yi, S.W.; Miao, X.D.; Vandenberghe, J.; Li, Y.Q.; Lu, H.Y. Late Quaternary aggradation and incision in the headwaters of the Yangtze River, eastern Tibetan Plateau, China. *Geol. Soc. Am. Bull.* **2022**, *134*, 371–388. [[CrossRef](#)]
10. Schumm, S.A. *The Fluvial System*; John Wiley: New York, NY, USA, 1977.
11. Vandenberghe, J. The fluvial cycle at cold–warm–cold transitions in lowland regions: A refinement of theory. *Geomorphology* **2008**, *98*, 275–284. [[CrossRef](#)]
12. Larkin, Z.T.; Ralph, T.J.; Tooth, S.; Duller, G.A.T. A shifting 'river of sand': The profound response of Australia's Warrego River to Holocene hydroclimatic change. *Geomorphology* **2020**, *370*, 107385. [[CrossRef](#)]
13. Tao, Y.L.; Xiong, J.G.; Zhang, H.P.; Chang, H.; Li, L.Y. Climate-driven formation of fluvial terraces across the Tibetan Plateau since 200 ka: A review. *Quat. Sci. Rev.* **2020**, *237*, 106303. [[CrossRef](#)]
14. Gao, H.S.; Li, Z.M.; Liu, X.F.; Pan, B.T.; Wu, Y.J.; Liu, F.L. Fluvial terraces and their implications for Weihe River valley evolution in the Sanyangchuan Basin. *Sci. China Earth Sci.* **2017**, *60*, 413–427. [[CrossRef](#)]
15. Maddy, D.; Veldkamp, A.; Demir, T.; van Gorp, W.; Wijbrans, J.R.; van Hinsbergen, D.J.J.; Dekkers, M.J.; Schreve, D.; Schoorl, J.M.; Scaife, R.; et al. The Gediz River fluvial archive: A benchmark for Quaternary research in Western Anatolia. *Quat. Sci. Rev.* **2017**, *166*, 289–306. [[CrossRef](#)]
16. Wang, X.Y.; Vandenberghe, J.; Lu, H.Y.; Van Balen, R. Climatic and tectonic controls on the fluvial morphology of the Northeastern Tibetan Plateau (China). *J. Geogr. Sci.* **2017**, *27*, 1325–1340. [[CrossRef](#)]
17. Gao, H.S.; Li, Z.M.; Pan, B.T.; Liu, F.L.; Liu, X.P. Fluvial responses to late Quaternary climate change in the Shiyang River drainage system, western China. *Geomorphology* **2016**, *258*, 82–94. [[CrossRef](#)]
18. Kalicki, T.; Kalicki, P. Fluvial activity in the Lomas de Lachay during the upper Pleistocene and Holocene. *Geomorphology* **2020**, *357*, 107087. [[CrossRef](#)]
19. Sinha, R.; Singh, A.; Tandon, S.K. Fluvial archives of north and northwestern India as recorders of climatic signatures in the late Quaternary: Review and assessment. *Curr. Sci. India* **2020**, *119*, 232–243. [[CrossRef](#)]
20. Knox, J.C. Valley alluviation in Southwestern Wisconsin. *Ann. Assoc. Am. Geogr.* **1972**, *62*, 401–410. [[CrossRef](#)]
21. Vandenberghe, J. Time scales, climate and river development. *Quat. Sci. Rev.* **1995**, *14*, 631–638. [[CrossRef](#)]
22. Blum, M.D.; Toomey III, R.S.; Valastro, S., Jr. Fluvial response to Late Quaternary climatic and environmental change, Edwards Plateau, Texas. *Palaeogeogr. Palaeoclimatol. Palaeoecol.* **1994**, *108*, 1–21. [[CrossRef](#)]
23. Knox, J.C. Late Quaternary Upper Mississippi River alluvial episodes and their significance to the Lower Mississippi River system. *Eng. Geol.* **1996**, *45*, 263–285. [[CrossRef](#)]

24. Wang, X.Y.; Vandenberghe, J.; Yi, S.W.; Van Balen, R.; Lu, H.Y. Climate-dependent fluvial architecture and processes on a suborbital timescale in areas of rapid tectonic uplift: An example from the NE Tibetan Plateau. *Glob. Planet. Change* **2015**, *133*, 318–329. [[CrossRef](#)]
25. Xu, L.X.; Ran, Y.K.; Liu, H.G.; Li, A. ¹⁰Be-derived sub-Milankovitch chronology of Late Pleistocene alluvial terraces along the piedmont of SW Tian Shan. *Geomorphology* **2019**, *328*, 173–182. [[CrossRef](#)]
26. Jain, M.; Tandon, S.K. Fluvial response to Late Quaternary climate changes, western India. *Quat. Sci. Rev.* **2003**, *22*, 2223–2235. [[CrossRef](#)]
27. Zheng, J.Y.; Yin, Y.H.; Li, B.Y. A new scheme for climate regionalization in China. *Acta. Geogr. Sin.* **2010**, *65*, 3–12. (In Chinese)
28. Zhang, B.P. Ten major scientific issues concerning the study of China's North-South Transitional Zone. *Progr. Geogr.* **2019**, *38*, 305–311. (In Chinese)
29. Ning, Y.; Qian, M.; Wang, Y.T. *Hydrology Handbook of the Huaihe River Drainage Basin*; Science Press: Beijing, China, 2003. (In Chinese)
30. Xu, J.X. Morphological analysis of flood of the Huai River. *J. Catastrophol.* **1992**, *7*, 45–50. (In Chinese)
31. Zhao, X.T.; Tang, L.Y.; Shen, C.M.; Wang, S.H. Climate evolution and sea level changes based on Qingfeng Section, Jianhu, Jiangsu. *Acta Oceanol. Sin.* **1994**, *16*, 78–88. (In Chinese)
32. Li, X.Y.; Huang, C.C.; Pang, J.L.; He, Z. Dust source of the Holocene loess soil and pedogenic environmental changes in the upper Huaihe River. *J. Geogr. Sci.* **2009**, *19*, 107–117. [[CrossRef](#)]
33. Yang, J.F.; Hou, L.X.; Chao, H.L.; Zeng, X.Y.; Jiao, J.H. Climate and basin evolution in the southwestern Huanghuai Plain from 130 to 13 ka: A case study of the Huzupu profile in Xinyang, Henan Province. *Acta Geol. Sin. Henan* **2011**, *1*, 20–25. (In Chinese)
34. Li, K.F.; Gao, W.H. Holocene climate change in Henan area: A synthesis of proxy records. *Quat. Int.* **2019**, *521*, 185–193. [[CrossRef](#)]
35. Li, Z.M.; Zhu, W.M.; Gao, H.S.; Liu, F.L.; Xing, W. Late Cenozoic climate changes in the Huanghuai Plain. *Mar. Geol. Quat. Geol.* **2021**, *41*, 179–191. (In Chinese)
36. Liu, Y.; Yang, P.P.; Shu, Q. Paleoclimatic and paleoenvironmental changes in late stage of late Pleistocene inferred from lacustrine sediment in Subei basin. *Earth Env.* **2021**, *49*, 1–8. (In Chinese)
37. Chen, J.R.; Shu, Q.; Zhao, Z.J.; Zhang, M.H. Climate change records of lacustrine deposits of Subei Basin in eastern China, 30–17 cal ka BP. *Geol. Sci. Tech. Inf.* **2017**, *36*, 75–79. (In Chinese)
38. Stuiver, M.; Grootes, P.M.; Braziunas, T.F. The GISP2 $\delta^{18}\text{O}$ climate record of the past 16,500 years and the role of the sun, ocean, and volcanoes. *Quat. Res.* **1995**, *44*, 341–354. [[CrossRef](#)]
39. Wang, Y.J.; Cheng, H.; Edwards, R.L.; An, Z.S.; Wu, J.Y.; Shen, C.C.; Dorale, J.A. A High-Resolution Absolute-Dated Late Pleistocene Monsoon Record from Hulu Cave, China. *Science* **2001**, *294*, 2345–2348. [[CrossRef](#)]
40. Wang, Y.J.; Cheng, H.; Edwards, R.L.; Kong, X.G.; Shao, X.H.; Chen, S.T.; Wu, J.Y.; Jiang, X.Y.; Wang, X.F.; An, Z.S. Millennial- and orbital-scale changes in the East Asian monsoon over the past 224,000 years. *Nature* **2008**, *451*, 1090–1093. [[CrossRef](#)] [[PubMed](#)]
41. Mao, R.X.; Cai, Y.J.; Ma, L.; Cheng, X. Early to mid-Holocene paleoclimatic changes recorded by the stalagmites from the Magou Cave, Henan Province. *J. Earth Env.* **2016**, *7*, 254–268. (In Chinese)
42. Hao, Z.X.; Zheng, J.Y.; Ge, Q.S.; Zhang, X.Z. Spatial patterns of precipitation anomalies for 30-yr warm periods in China during the past 2000 years. *Acta. Meteorol. Sin.* **2012**, *26*, 278–288. [[CrossRef](#)]
43. Chen, J.H.; Chen, F.H.; Feng, S.; Huang, W.; Liu, J.B.; Zhou, A.F. Hydroclimatic changes in China and surroundings during the Medieval Climate Anomaly and Little Ice Age: Spatial patterns and possible mechanisms. *Quat. Sci. Rev.* **2015**, *107*, 98–111. [[CrossRef](#)]
44. Zhou, X.C.; Jiang, D.B.; Lang, X.M. A multi-model analysis of 'Little Ice Age' climate over China. *Holocene* **2019**, *29*, 592–605. [[CrossRef](#)]
45. Qin, X.G.; Zhang, L.; Mu, Y. The Holocene climatic changes of the Huaihe River semi-humid region in the North and South Transition Zone of the eastern China. *Quat. Sci.* **2015**, *35*, 1509–1524. (In Chinese)
46. Shu, Q.; Zhao, Z.J.; Chen, Y.; Zhang, M.H.; Li, J.J. Palaeoenvironmental significance of geochemistry elements and grain size of DS core sediments in Xinghua, Jiangsu Province. *Sci. Geogr. Sini.* **2009**, *29*, 923–928. (In Chinese)
47. Shu, Q.; Chen, Y.; Zhao, Z.J.; Zhang, M.H. Paleoclimatic and paleoenvironmental evolution since the Late Glacial epoch in Jianghuai Plain. *Sci. Geogr. Sin.* **2013**, *33*, 1377–1382. (In Chinese) [[CrossRef](#)]
48. Chen, F.H.; Yu, Z.C.; Yang, M.L.; Ito, E.; Wang, S.M.; Madsen, D.B.; Huang, X.Z.; Zhao, Y.; Sato, T.; Birks, H.J.B.; et al. Holocene moisture evolution in arid central Asia and its out-of-phase relationship with Asian monsoon history. *Quat. Sci. Rev.* **2008**, *27*, 351–364. [[CrossRef](#)]
49. Chen, F.H.; Jia, J.; Chen, J.H.; Li, G.Q.; Zhang, X.J.; Xie, H.C.; Xia, D.S.; Huang, W.; An, C.B. A persistent Holocene wetting trend in arid central Asia, with wettest conditions in the late Holocene, revealed by multi-proxy analyses of loess-paleosol sequences in Xinjiang, China. *Quat. Sci. Rev.* **2016**, *146*, 134–146. [[CrossRef](#)]
50. Yang, X.P.; Liang, P.; Zhang, D.G.; Li, H.W.; Rioual, P.; Wang, X.L.; Xu, B.; Ma, Z.B.; Liu, Q.Q.; Ren, X.Z.; et al. Holocene aeolian stratigraphic sequences in the eastern portion of the desert belt (sand seas and sandy lands) in northern China and their palaeoenvironmental implications. *Sci. China Earth Sci.* **2019**, *62*, 1302–1315. [[CrossRef](#)]
51. Reimer, P.J.; Bard, E.; Bayliss, A.; Beck, W.; Blackwell, P.G.; Ramsey, C.B.; Brown, D.M.; Buck, C.E.; Edwards, R.L.; Friedrich, M.; et al. Selection and treatment of data for radiocarbon calibration: An update to the international calibration (INTCAL) criteria. *Radiocarbon* **2013**, *55*, 1923–1945. [[CrossRef](#)]

52. Lai, Z.P.; Wintle, A.G. Locating the boundary between the Holocene and Pleistocene In Chinese loess using luminescence. *Holocene* **2006**, *16*, 893–899. [[CrossRef](#)]
53. Roberts, H.M. Assessing the effectiveness of the double-SAR protocol in isolating a luminescence signal dominated by quartz. *Radiat. Meas.* **2007**, *42*, 1627–1636. [[CrossRef](#)]
54. Murray, A.S.; Wintle, A.G. Luminescence dating of quartz using an improved single-aliquot regenerative-dose protocol. *Radiat. Meas.* **2000**, *32*, 57–73. [[CrossRef](#)]
55. Roberts, H.M.; Duller, G.A.T. Standardised growth curves for optical dating of sediment using multiple-grain aliquots. *Radiat. Meas.* **2004**, *38*, 241–252. [[CrossRef](#)]
56. Lai, Z.P. Testing the use of an OSL standardised growth curve (SGC) for De de-termination on quartz from the Chinese Loess Plateau. *Radiat. Meas.* **2006**, *41*, 9–16. [[CrossRef](#)]
57. Lai, Z.P.; Brückner, H.; Zöller, L.; Fülling, A. Existence of a common growth curve for silt-sized quartz OSL of loess from different continents. *Radiat. Meas.* **2007**, *42*, 1432–1440. [[CrossRef](#)]
58. Prescott, J.R.; Hutton, J.T. Cosmic ray contributions to dose rates for luminescence and ESR dating: Large depths and long-term time variations. *Radiat. Meas.* **1994**, *23*, 497–500. [[CrossRef](#)]
59. Singarayer, J.S.; Bailey, R.M. Further investigations of the quartz optically stimulated luminescence components using linear modulation. *Radiat. Meas.* **2003**, *37*, 451–458. [[CrossRef](#)]
60. Makaske, B. Anastomosing rivers: A review of their classification, origin and sedimentary products. *Earth Sci. Rev.* **2001**, *53*, 149–196. [[CrossRef](#)]
61. Nanson, G.C. Anabranching and Anastomosing Rivers. In *Treatise on Geomorphology*; Wohl, E., Ed.; Fluvial Geomorphology; Academic Press: San Diego, CA, USA, 2013; Volume 9, pp. 330–345.
62. Miall, A.D. The Geology of Fluvial Deposits. In *Sedimentary Facies, Basin Analysis, and Petroleum Geology*; Springer: Berlin/Heidelberg, Germany, 1996.
63. Wang, X.Y.; Ma, J.F.; Yi, S.W.; Vandenberghe, J.; Dai, Y.; Lu, H.Y. Interaction of fluvial and eolian sedimentation processes, and response to climate change since the last glacial in a semiarid environment along the Yellow River. *Quat. Res.* **2018**, *91*, 570–583. [[CrossRef](#)]
64. Huang, X.Y.; Meyers, P.A.; Jia, C.L.; Zheng, M.; Xue, J.T.; Wang, X.X.; Xie, S.C. Paleotemperature variability in central China during the last 13 ka recorded by a novel microbial lipid proxy in the Dajiuhe peat deposit. *Holocene* **2013**, *23*, 1123–1129. [[CrossRef](#)]
65. Ge, Q.S.; Zheng, J.Y.; Hao, Z.X.; Shao, X.M.; Wang, W.C.; Luterbacher, J. Temperature variation through 2000 years in China: An uncertainty analysis of reconstruction and regional difference. *Geophys. Res. Lett.* **2010**, *37*, L03703. [[CrossRef](#)]
66. Ge, Q.S.; Zheng, J.Y.; Hao, Z.X.; Liu, H.L. General characteristics of climate changes during the past 2000 years in China. *Sci. China Earth Sci.* **2013**, *56*, 321–329. [[CrossRef](#)]
67. Ge, Q.S. *Climate Change in Chinese Dynasties*; Science Press: Beijing, China, 2011. (In Chinese)
68. Wu, H.; Li, Q.; Yu, Y.; Sun, A.; Lin, Y.; Jiang, W.; Luo, Y. Quantitative climatic reconstruction of the Last Glacial Maximum in China. *Sci. China Earth Sci.* **2019**, *62*, 1269–1278. [[CrossRef](#)]
69. Li, M.; Zhang, S.; Xu, Q.; Xiao, J.; Wen, R. Spatial patterns of vegetation and climate in the North China Plain during the Last Glacial Maximum and Holocene climatic optimum. *Sci. China Earth Sci.* **2018**, *62*, 1279–1287. [[CrossRef](#)]
70. Hu, X.F.; Pan, B.T.; Gao, H.S.; Cao, B.; Li, Q.Y.; Geng, H.P. Development of Holocene fluvial terraces in the eastern Qilianshan Mountain and its relationship with climatic changes. *Quat. Sci.* **2013**, *33*, 723–736. (In Chinese)
71. Nordt, L. Late Quaternary alluvial stratigraphy of a low-order tributary in central Texas, USA and its response to climate and sediment supply. *Quat. Res.* **2004**, *62*, 289–300. [[CrossRef](#)]
72. Macklin, M.G.; Benito, G.; Gregory, K.J.; Johnstone, E.; Lewin, J.; Michczyńska, D.J.; Soja, R.; Starkel, L.; Thorndycraft, V.R. Past hydrological events reflected in the Holocene fluvial record of Europe. *Catena* **2006**, *66*, 145–154. [[CrossRef](#)]
73. Chiriloaei, F.; Rădoane, M.; Perşoiu, I.; Popa, I. Late Holocene history of the Moldova River Valley, Romania. *Catena* **2012**, *93*, 64–77. [[CrossRef](#)]
74. Barros, L.F.P.; Magalhães, A.P., Jr. Late quaternary landscape evolution in the Atlantic Plateau (Brazilian highlands): Tectonic and climatic implications of fluvial archives. *Earth Sci. Rev.* **2020**, *207*, 103228. [[CrossRef](#)]
75. Chen, G.; Zheng, W.J.; Xiong, J.G.; Zhang, P.Z.; Li, Z.G.; Yu, J.X.; Li, X.N.; Wang, Y.; Zhang, Y.P. Late Quaternary fluvial landform evolution and controlling factors along the Yulin River on the Northern Tibetan Plateau. *Geomorphology* **2020**, *363*, 107213. [[CrossRef](#)]
76. Van Huissteden, J.; Kasse, C. Detection of rapid climate change in the Last Glacial fluvial successions in The Netherlands. *Glob. Planet. Chang.* **2001**, *28*, 319–339. [[CrossRef](#)]
77. Kasse, C.; Vandenberghe, J.; Van Huissteden, J.; Bohncke, S.J.P.; Bos, J.A.A. Sensitivity of Weichselian fluvial systems to climate change (Nochten mine, eastern Germany). *Quat. Sci. Rev.* **2003**, *22*, 2141–2156. [[CrossRef](#)]
78. Kasse, C.; Bohncke, S.J.P.; Vandenberghe, J.; Gábris, G. Fluvial style changes during the last glacial–interglacial transition in the middle Tisza valley (Hungary). *Proc. Geol. Assoc.* **2010**, *121*, 180–194. [[CrossRef](#)]
79. Leigh, D.S. Late Quaternary climates and river channels of the Atlantic Coastal Plain, Southeastern USA. *Geomorphology* **2008**, *101*, 90–108. [[CrossRef](#)]
80. Fitzsimmons, K.E.; Cohen, T.J.; Hesse, P.P.; Jansen, J.; Nanson, G.C.; May, J.H.; Barrows, T.T.; Haberlah, D.; Hilgers, A.; Kelly, T.; et al. Late Quaternary palaeoenvironmental change in the Australian drylands. *Quat. Sci. Rev.* **2013**, *74*, 78–96. [[CrossRef](#)]

81. Nanson, G.C.; Price, D.M.; Jones, B.G.; Maroulis, J.C.; Coleman, M.; Bowman, H.; Cohen, T.J.; Pietsch, T.J.; Larsen, J.R. Alluvial evidence for major climate and flow regime changes during the middle and late Quaternary in eastern central Australia. *Geomorphology* **2008**, *101*, 109–129. [[CrossRef](#)]
82. Wesnousky, S.G.; Owen, L.A. Development of the Truckee River terraces on the northeastern flank of the Sierra Nevada. *Geomorphology* **2020**, *370*, 107399. [[CrossRef](#)]

Disclaimer/Publisher’s Note: The statements, opinions and data contained in all publications are solely those of the individual author(s) and contributor(s) and not of MDPI and/or the editor(s). MDPI and/or the editor(s) disclaim responsibility for any injury to people or property resulting from any ideas, methods, instructions or products referred to in the content.